Turbulent Liquid," *Chem. Eng. Sci.*, **27**, 1035 (1972).
Lynn, S., J. R. Straatmeir, and H. Kramers, "Absorption Studies in the Light of the Penetration Theory I. Long Wetted-Wall Columns," *ibid.*, **4**, 49 (1955).
Méndez, F. "Gas Absorption Accompanied by Instantaneous Bimolecular Reaction in Turbulent Liquids," M.S. thesis, Univ. California, Santa Barbara (1973).
Menez, G. D., and O. C. Sandall, "Gas Absorption Accompanied by First Order Chemical Reaction in Turbulent Liquids," *Ind. Eng. Chem. Fundamentals*, **13**, 72 (1974).
Mills, A. F., and D. K. Chung, "Heat Transfer Across Falling Films," *Intern. J. Heat Mass Transfer*, **16**, 694 (1973).
Nijsing, R.A.T.O., and H. Kramers, "Absorption of CO_2 in Carbonate Bicarbonate Buffer Solutions in a Wetted Wall Column," p. 81, 1st Eur. Symp. Chem. React. Eng., Amsterdam (1957).
Perez, J. F., and O. C. Sandall, "Diffusivity Measurements for Gases in Power Law Non-Newtonian Liquids," *AIChE J.*, **19**, 1073 (1973).
Perry, R. H., C. H. Chilton, and C. H. Kirkpatrick, (ed)., *Perry's Chemical Engineers' Handbook*, 4th edit., pp 14-41, McGraw-Hill, New York (1963).
Sandall, O. C., "Gas Absorption into Turbulent Liquids at Intermediate Contact Times," *Intern. J. Heat Mass Transfer*, **17**, 459 (1974).
Vivian, J. E., and C. J. King, "Diffusivities of Slightly Soluble Gases in Water," *AIChE J.*, **10**, 220 (1964).

Manuscript received June 3, 1974; revision received December 2 and accepted December 4, 1974.

The Behavior of a Power-Law Fluid Flowing Through a Sudden Expansion:

Part I. A Numerical Solution

A numerical solution for the axisymmetric flow of an inelastic power-law fluid through an abrupt circular expansion is presented. The equations of motion were solved using an Alternating Direction Implicit method. Both a stream tube-real tube and a real tube-real tube model were investigated and the conditions for significant upstream diffusion of momentum were specified. Secondary flow characteristics and the bulk flow field development are predicted as a function of the flow behavior index (n) and of the Reynolds number. Some results are presented to show the influence of the expansion ratio.

A. L. HALMOS
D. V. BOGER
Department of Chemical Engineering
Monash University
Clayton, Victoria, Australia

and

A. CABELLI
Division of Mechanical Engineering
C.S.I.R.O.
Highett, Victoria, Australia

SCOPE

The flow of inelastic power-law fluids through sudden circular expansions is not a problem of great commercial significance in its own right, but this flow field must be understood before the flow of the more complex viscoelastic fluid can be examined. The viscoelastic fluid in abruptly expanding flow fields is of considerable importance in polymer melt processing.

Only one numerical solution, which is confined to Newtonian fluids, is available in the literature. No experimental data for inelastic or viscoelastic fluids are available. The object of this work is to present an experimentally verified numerical solution of the equations of motion for flow of inelastic power-law fluids in abrupt circular expansions.

The numerical solution was obtained using an Alternating Direction Implicit method. Both a stream tube-real tube and a real tube-real tube model were investigated. The conditions for significant diffusion of momentum upstream of the plane of expansion are specified. Eddy characteristics and flow field development are predicted as functions of the flow behavior index n and of the Reynolds number. Some results showing the influence of the expansion ratio are presented. Experimental data are presented to verify the numerical model. Streak photography was used for recording flow patterns and a multiple flash technique was used for point velocity measurement. Fluid properties were determined with an R16 Weissenberg Rheogoniometer. The measured reattachment lengths, the recorded flow patterns, and the developing axial velocity field all show excellent agreement with the numerical predictions.

A. L. Halmos is with the Department of Chemical Engineering and Chemical Technology, Imperial College, London SW7 2AZ, England.

CONCLUSIONS AND SIGNIFICANCE

A numerical solution of the equations of motion was obtained for inelastic fluids flowing through abrupt circular expansions. The Alternating Direction Implicit method used was found to be a satisfactory method of solution for this nonlinear, open-ended problem for a Reynolds number range of 0 to 150 and for a flow behavior index range of 0.65 to 1.00. Excellent agreement was obtained with the numerical work of Macagno and Hung (1967) for Newtonian fluids.

Two models were investigated: a stream tube-real tube and a real tube-real tube model. The latter allowed for diffusion of momentum upstream from the plane of expansion, while the former imposed fully developed flow at the expansion mouth. Diffusion of momentum upstream from the expansion was found to be negligible for $Re_{\text{mod}} \geq 20$ and for $n \leq 1.00$. The stream tube-real tube model was therefore applicable for $Re_{\text{mod}} \geq 20$ and the real tube-real tube model for $Re_{\text{mod}} < 20$.

The secondary cell produced in the corner of the expansion was found to have a buffering effect on the decelerating flow. As the Reynolds number increases at constant flow behavior index, the size of the secondary cell increases, greater energy is dissipated in the cell and deceleration is more gradual. As the flow behavior index decreases ($n \leq 1.00$) at constant Reynolds number, the size of the secondary cell increases and deceleration is again more gradual. At constant values of the flow behavior index, the intensity of the secondary cell increases with increasing Reynolds number because of the greater momentum imparted to the eddy. At constant values of the Reynolds number, the intensity decreases with decreasing power-law index because of an increasing apparent viscosity in the cell. Increasing the expansion ratio from 1.5 up to 4 causes all effects to be magnified.

Streak photography was used for recording flow patterns and a multiple flash technique was developed and proven for point velocity measurement. Fundamental flow properties of the test fluids were measured using an R16 Weissenberg Rheogoniometer in the cone and plate configuration. Experimental work was confined to a 1 to 2 expansion with a Reynolds number and a flow behavior index which varied from 6.7 to 158.8 and from 0.65 to 0.81, respectively. The measured reattachment length of the secondary cell which was formed in the corner of the expansion, the recorded streamlines, and the measured values of the developing axial velocity field all showed excellent agreement with the numerical predictions.

An experimentally verified numerical model for flow of inelastic power-law fluids through abrupt circular expansions is now available and the details of the secondary and bulk flows are understood.

GOVERNING DIFFERENTIAL EQUATIONS

The isothermal flow of an incompressible fluid through an abrupt axisymmetric expansion (Figure 1) is described by

$$\frac{1}{r}\frac{\partial(ur)}{\partial r} + \frac{\partial v}{\partial z} = 0 \tag{1}$$

$$\rho\frac{Du}{Dt} = -\frac{\partial P}{\partial r} - \left(\frac{1}{r}\frac{\partial}{\partial r}(r\tau'_{rr}) + \frac{\tau'_{\theta\theta}}{r} + \frac{\partial \tau'_{rz}}{\partial z}\right) \tag{2}$$

$$\rho\frac{Dv}{Dt} = -\frac{\partial P}{\partial z} - \left(\frac{1}{r}\frac{\partial}{\partial r}(r\tau'_{rz}) + \frac{\partial \tau'_{zz}}{\partial z}\right) \tag{3}$$

where

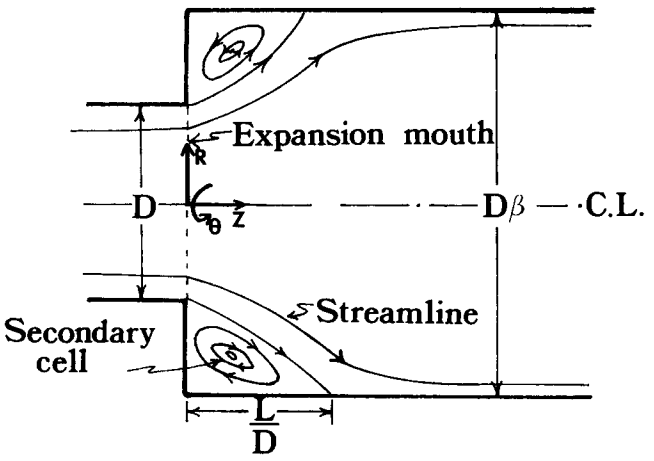

Fig. 1. Diagram of flow through an abrupt circular expansion.

$$\frac{D}{Dt} = \frac{\partial}{\partial t} + u\frac{\partial}{\partial r} + v\frac{\partial}{\partial z} \tag{4}$$

is the substantial time derivative, u and v are, respectively, the radial and axial components of velocity. Cross differentiating Equations (2) and (3) to eliminate the pressure yields

$$\rho\left(\frac{D\eta'}{Dt} - \frac{u\eta'}{r}\right) = \frac{\partial^2\tau'_{rz}}{\partial r^2} + \frac{1}{r}\frac{\partial \tau'_{rz}}{\partial r} - \frac{\tau'_{rz}}{r^2} + \frac{\partial^2\tau'_{zz}}{\partial r\partial z} - \frac{\partial^2\tau'_{rr}}{\partial r\partial z} - \frac{1}{r}\frac{\partial \tau'_{rr}}{\partial z} + \frac{1}{r}\frac{\partial \tau'_{\theta\theta}}{\partial z} - \frac{\partial \tau'_{rz}}{\partial z^2} \tag{5}$$

where η' is the vorticity defined by

$$\eta' = \frac{\partial u}{\partial z} - \frac{\partial v}{\partial r} \tag{6}$$

The generalized Oswald-de Waele model (power-law) (Bird et al., 1960) was used to relate the local stress to the local rate of deformation. It describes an inelastic, time independent, isotropic fluid which exhibits no yield stress. The nonzero stresses can then be defined by

$$\left.\begin{aligned}
\tau'_{rz} &= -k\phi'\left(\frac{\partial u}{\partial z} + \frac{\partial v}{\partial r}\right)\\
\tau'_{rr} &= -2k\phi'\frac{\partial u}{\partial r}\\
\tau'_{zz} &= -2k\phi'\frac{\partial v}{\partial z}\\
\tau'_{\theta\theta} &= -2k\phi'\frac{u}{r}
\end{aligned}\right\} \tag{7}$$

where ϕ' is the apparent viscosity given by

$$\phi' = \left| 2\left\{ \left(\frac{\partial u}{\partial r}\right)^2 + \left(\frac{u}{r}\right)^2 + \left(\frac{\partial v}{\partial z}\right)^2 \right\} + \left(\frac{\partial v}{\partial r} + \frac{\partial u}{\partial z}\right)^2 \right|^{(n-1)/2} \quad (8)$$

n is the flow behavior index and k is the consistency factor.

Introducing the dimensionless variables given by

$$R = \frac{r}{D}, \quad Z = \frac{z}{D}, \quad U = \frac{u}{W}, \quad V = \frac{v}{W}$$

$$\text{and} \quad \tau = \tau'\left(\frac{D}{W}\right)^n \frac{1}{k} \quad (9)$$

where D and W are the tube diameter and average velocity upstream of the expansion respectively, then

$$\eta = \eta'\left(\frac{D}{W}\right), \quad \phi = \phi'\left(\frac{D}{W}\right)^{n-1},$$

$$\frac{D}{DT} = \frac{W}{D}\frac{D}{Dt}, \quad \tau_{RR} = 2\phi\frac{\partial U}{\partial R} \quad \text{etc.}$$

$$\text{and} \quad T = t\left(\frac{D}{W}\right) \quad (10)$$

The dimensionless equation which corresponds to Equation (8) is

$$\phi = \left| 2\left\{ \left(\frac{\partial U}{\partial R}\right)^2 + \left(\frac{U}{R}\right)^2 + \left(\frac{\partial V}{\partial Z}\right)^2 \right\} + \left(\frac{\partial V}{\partial R} + \frac{\partial U}{\partial Z}\right)^2 \right|^{(n-1)/2} \quad (8a)$$

Equation (5) then reduces to

$$\frac{D\eta}{DT} - \frac{U\eta}{R} = \left(\frac{k}{\rho D^n W^{2-n}}\right)\left(\phi\left(\nabla^2\eta - \frac{\eta}{R^2}\right) + \frac{\partial\phi}{\partial R}\left(\frac{\eta}{R} + 2\frac{\partial\eta}{\partial R}\right) + 2\frac{\partial\phi}{\partial Z}\frac{\partial\eta}{\partial Z} + \left(\frac{\partial U}{\partial Z} + \frac{\partial V}{\partial R}\right)\left(\frac{\partial^2\phi}{\partial Z^2} - \frac{\partial^2\phi}{\partial R^2}\right) + 2\frac{\partial^2\phi}{\partial R\partial Z}\left(\frac{\partial U}{\partial Z} - \frac{\partial V}{\partial Z}\right)\right) \quad (11)$$

where

$$\eta = \frac{\partial U}{\partial Z} - \frac{\partial V}{\partial R} \quad (12)$$

and

$$\nabla^2 = \frac{\partial^2}{\partial R^2} + \frac{\partial^2}{\partial Z^2} + \frac{1}{R}\frac{\partial}{\partial R} \quad (13)$$

Equation (11) collapses to the appropriate Navier-Stokes equation for $n = 1$ (Hung, 1966). The group $(\rho D^n W^{2-n})/k$ represents a modified Reynolds number which may be derived by dimensional analysis and differs from the generalized Reynolds number (Skelland, 1967) by the absence of the factor $\left(8^{(1-n)}\left(\frac{4n}{3n+1}\right)^n\right)$.

The equation of continuity [Equation (3)] is satisfied by defining the stream function, ψ as

$$U = \frac{1}{R}\frac{\partial\psi}{\partial Z}, \quad V = -\frac{1}{R}\frac{\partial\psi}{\partial R} \quad (14)$$

and Equation (12) then becomes

$$\eta = \frac{1}{R}\left(\nabla^2\psi - \frac{2}{R}\frac{\partial\psi}{\partial R}\right) \quad (15)$$

The flow of an inelastic power-law fluid through an abrupt expansion is then described by Equations (11), (14), (15), and (8a).

Two models of the expansion flow were formulated: a Stream Tube-Real Tube (ST-RT) and a Real Tube-Real Tube (RT-RT) model. In the ST-RT model it is assumed that there is no axial diffusion of momentum upstream of the plane of the expansion and therefore that the flow field upstream of the expansion is unaffected by the expansion itself. Prandtl (1952) defined the stream tube as a tube where the flow is always tangential to the wall. A fully developed velocity profile is therefore specified at the mouth of the expansion. In the RT-RT model predevelopment of the flow field is allowed by imposing the fully developed velocity profile far upstream of the expansion mouth. The ST-RT model is the simpler approach but can only be used with certainty after the significance of upstream axial diffusion of momentum is determined by use of the RT-RT model.

BOUNDARY CONDITIONS

RT-RT Model

(i) $R = \frac{1}{2}$, $Z \leq 0$ and $R = \beta/2$, $Z \geq 0$ (horizontal solid boundaries)

$$U = V = \frac{\partial U}{\partial Z} = \frac{\partial V}{\partial Z} = \frac{\partial\psi}{\partial R} = 0 \quad (16)$$

$$\psi = 0 \quad \text{(arbitrary definition)} \quad (17)$$

$$\eta = -\frac{\partial V}{\partial R} \quad (18)$$

$$\phi = \left| 2\left(\frac{\partial U}{\partial R}\right)^2 + \left(\frac{\partial V}{\partial R}\right)^2 \right|^{(n-1)/2} \quad (19)$$

(ii) $R = 0$ (tube centerline)

$$U = \eta = \frac{\partial U}{\partial Z} = \frac{\partial V}{\partial R} = \frac{\partial\psi}{\partial R} = 0 \quad (20)$$

$$V = \lim_{R\to 0}\left(-\frac{1}{R}\frac{\partial\psi}{\partial R}\right) = -\frac{\partial^2\psi}{\partial R^2} \quad (21)$$

$$\psi = \frac{1}{8} \quad (22)$$

$$\phi = \left| 4\left(\frac{\partial U}{\partial R}\right)^2 + 2\left(\frac{\partial V}{\partial Z}\right)^2 \right|^{(n-1)/2} \quad (23)$$

$$\text{Since} \left(\lim_{R\to 0}\frac{U}{R} = \frac{\partial U}{\partial R}\right)$$

(iii) $Z = -\infty$, $0 < R < \frac{1}{2}$

$$U = \frac{\partial U}{\partial R} = \frac{\partial U}{\partial Z} = \frac{\partial V}{\partial Z} = 0 \quad (24)$$

$$V = \left(\frac{3n+1}{n+1}\right)(1-(2R)^{(n+1)/n}) \quad (25)$$

$$\eta = \left(\frac{3n+1}{n}\right)2^{(n+1)/n}R^{1/n} \quad (26)$$

$$\psi = \frac{1}{8} - \left(\frac{3n+1}{n+1}\right)\left(\frac{R^2}{2} - \left(\frac{n}{3n+1}\right)2^{(n+1)/n}R^{(3n+1)/n}\right) \quad (27)$$

$$\phi = |\eta|^{n-1} \quad (28)$$

(iv) $Z = +\infty, \quad 0 < R < \beta/2$

$$U = \frac{\partial U}{\partial R} = \frac{\partial U}{\partial Z} = \frac{\partial V}{\partial Z} = 0 \quad (29)$$

$$V = \left(\frac{3n+1}{n+1}\right)\frac{1}{\beta^2}\left(1-\left(\frac{2R}{\beta}\right)^{(n+1)/n}\right) \quad (30)$$

$$\eta = \left(\frac{3n+1}{n}\right)2^{(n+1)/n}\left(\frac{1}{\beta}\right)^{(3n+1)/n}R^{1/n} \quad (31)$$

$$\psi = \frac{1}{8} - \left(\frac{3n+1}{n+1}\right)\left(\frac{1}{\beta^2}\right)\left(\frac{R^2}{2} - \left(\frac{n}{3n+1}\right)\left(\frac{2}{\beta}\right)^{(n+1)/n}R^{(n+1)/n}\right) \quad (32)$$

$$\phi = |\eta|^{n-1} \quad (33)$$

(v) $Z = 0, \quad \frac{1}{2} < R < \beta/2$

$$U = V = \frac{\partial U}{\partial R} = \frac{\partial V}{\partial R} = \frac{\partial V}{\partial Z} = 0 \quad (34)$$

$$\psi = 0 \quad \text{(arbitrary definition)} \quad (35)$$

$$\eta = \frac{\partial U}{\partial Z} \quad (36)$$

$$\phi = |\eta|^{n-1} \quad (37)$$

In the actual numerical solution the boundary conditions at $Z = \pm\infty$ were in fact imposed at finite distances from the expansion plane ($Z = 0$). A trial and error procedure was used to determine the minimum domain upstream and downstream from $Z = 0$ so that an invariant flow field was predicted. Axial coordinate transformations have been used (Vrentas et al., 1966; Christiansen et al., 1972) to map the infinite region to one of finite size. These transformations were not used here.

ST-RT Model

The boundary conditions are unchanged except for the imposition of a fully developed velocity profile at $Z = 0$ instead of $Z = -\infty$.

At $Z = 0, \quad 0 < R < \frac{1}{2}$

$$U = \frac{\partial U}{\partial R} = \frac{\partial V}{\partial Z} = 0 \quad (38)$$

$V =$ Equation (25)

$\psi =$ Equation (27)

$$\eta = \frac{\partial U}{\partial Z} + \left(\frac{3n+1}{n}\right)R^{(1/n)}2^{(n+1)/n} \quad (39)$$

$$\phi = \left|-\left(\frac{3n+1}{n}\right)2^{(n+1)/n}R^{1/n} + \frac{\partial V}{\partial Z}\right|^{n-1} \quad (40)$$

METHOD OF SOLUTION

The solution of primary interest is for the steady state behavior which may be described by leaving out the time-dependent term from Equation (11). The resulting equation is nonlinear and an analytical solution of it is not known. Boundary layer approaches are of little use in a problem where the properties of the secondary flow are of primary importance, and linearization techniques frequently necessitate approximations which oversimplify the equations to make them manageable and which, therefore, may obscure effects of considerable importance. A numerical technique was therefore used to solve the equations without further assumptions. The term including the partial derivative with respect to time was retained in Equation (11) and provided the means to obtain rapid convergence to the steady state solution.

Partial derivatives in the governing equations were approximated by finite difference expressions and the resulting relations were solved at the nodes of a grid superimposed on the solution domain. Second-order central differences were used to approximate the spatial derivatives of the velocities and the vorticity in Equations (11), (15), and (8a), while a fourth-order approximation was used for the derivatives of the stream function in the calculation of the velocity components from Equations (14), and fourth-order approximation was also used for the derivatives of the apparent viscosity and a first-order forward difference was used for the time derivative.

The Alternating Direction Implicit method (ADI), developed by Peaceman and Rachford (1955), was used for solution of Equation (11). In this technique the spatial derivatives of the dependent variable are specified implicitly in one coordinate direction and explicitly in the other direction. The solution progresses through half-time increments with the implicit and explicit directions reversed after each increment. When derivatives of order no greater than two are involved, tridiagonal matrices result. To represent the solution domain, up to 201 nodes were used in the axial direction and 11 in the radial direction. For each complete step forward in time this grid required the solution of 9 tridiagonal matrices (199×199) in the axial direction, and of 199 matrices (9×9) in the radial direction.

After each half-time increment, an updated estimate was made of the stream function by solving Equation (15). A point over-relaxation procedure was used (Smith, 1971) with the over-relaxation parameter being empirically varied in successive solution processes to minimize the required number of iterations (Cabelli, 1970). A relative convergence criterion was used to terminate this stage.

$$\sum_{\text{Solution domain}} \left|\frac{\psi_{\text{New}} - \psi_{\text{Old}}}{\psi_{\text{Old}}}\right| < \epsilon_\psi \quad \text{for} \quad \psi_{\text{Old}} \neq 0 \quad (41)$$

The convergence number ϵ_ψ was set equal to 0.1, but this was relaxed somewhat for the finer grids. Once the improved estimates for ψ were obtained, velocities were determined from Equation (14) and boundary values for the vorticity were found. Finally the apparent viscosity function [Equation (8a)] and its derivatives used in Equation (11) were calculated. These updated values for U, V, η (boundary), ϕ and the derivatives of ϕ were treated as constant parameters in the next step of the ADI solution of Equation (11). Douglas (1962) showed

that when a similar method is used, the overall accuracy improves from first to second order in time. An accelerated rate of convergence and a reduction in computation time of 10 to 15% was obtained by empirically varying the time step after each iteration (Cabelli, 1970).

Equation (11) was integrated until two convergence criteria were met:

$$\sum_{\text{Solution domain}} \left| \frac{\eta_{\text{New}} - \eta_{\text{Old}}}{\eta_{\text{Old}}} \right| < \epsilon_\eta \quad \text{for} \quad \eta_{\text{Old}} \neq 0 \quad (42)$$

$$\sum_{\text{Solution domain}} \left| \frac{U_{\text{New}} - U_{\text{Old}}}{U_{\text{Old}}} \right| < \epsilon_U \quad \text{for} \quad U_{\text{Old}} \neq 0 \quad (43)$$

The convergence numbers ϵ_η and ϵ_U were generally about 0.1. When the two criteria were satisfied, the solution was considered to have reached steady state.

The solution was initiated in either of two ways:

1. By linear interpolation of the stream function between the fully developed profiles at the two ends of the field, or
2. From a previously converged solution for minor differences in physical properties, the geometry, or the Reynolds number.

A problem arising from the use of the power-law model is concerned with evaluating the apparent viscosity at points where the velocity gradient approaches zero. As the velocity gradients tend to zero, the power-law model predicts an infinite apparent viscosity for $0 < n < 1$, which is not physically realistic. In the flow through an abrupt expansion, the velocity gradient becomes equal to zero at the center line where fully developed flow is approached and at the corner of the expansion ($Z = 0$, $R = \beta/2$). Gianquinta and Hung (1968), solving the problem of a two-dimensional expansion, mentioned this difficulty but did not explain how it was handled. Ozoe and Churchill (1972), who studied natural convection in non-Newtonian fluids heated from below, found that when an arbitrary value of 10^4 was assigned to the apparent viscosity at the critical points an unstable solution resulted. However, when each corner viscosity was assigned a value equal to the average of the values obtained by second-order extrapolation along both walls, a stable calculation resulted. In this work $\partial\phi/\partial R$ was evaluated analytically at the nodes adjacent to the critical points for both the ST-RT and the RT-RT models and was then differentiated numerically in the axial direction. The term $\partial^2\phi/\partial R\partial Z$ in Equation (11) could therefore be obtained at all interior nodes of the solution domain, and the need for the apparent viscosity at the three critical points was therefore eliminated. Much greater detail on all aspects of the numerical method are available elsewhere (Halmos, 1973a).

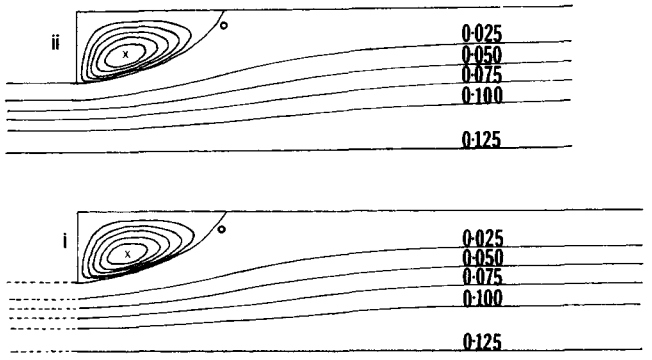

Fig. 2. Model comparison for stream function contours for $n = 0.75$, $Re_{mod} = 20$
(i) ST-RT model $\psi_{min} = -0.0058$
(ii) RT-RT model $\psi_{min} = -0.0061$

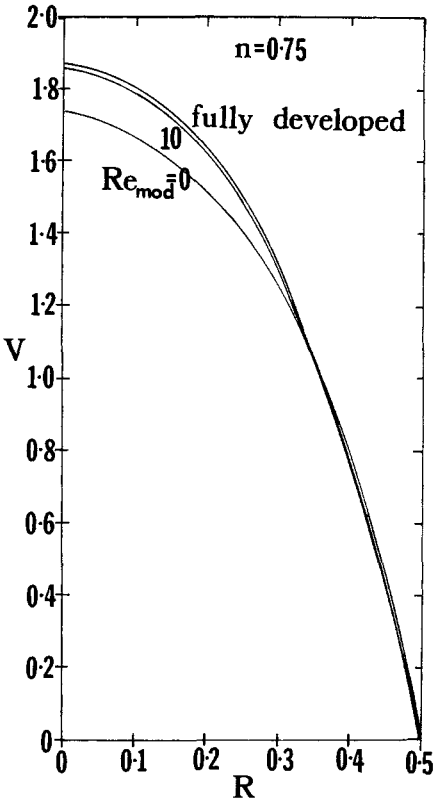

Fig. 3. Axial velocity profile for $n = 0.75$ at the expansion mouth for different Reynolds numbers.

NUMERICAL RESULTS AND DISCUSSIONS

Most results were obtained for a 1 to 2 expansion using a mesh size of 1/10 with 11 nodes in the radical direction. In the axial direction, the number of nodes was varied up to 201 depending on the magnitude of the modified Reynolds number and to a small extent on the magnitude of the power-law index. These aspects and the effect of the mesh size are discussed by Halmos (1973b).

The flow patterns generated in the 1-2 expansion are represented in Figure 2 where stream function profiles obtained by use of the ST-RT and RT-RT model are shown for $n = 0.75$ and $Re_{\text{mod}} = 20$. The center of the secondary cell is designated by an X which corresponds to the minimum value of the stream function. The contours are divided into equal increments from ⅛ at the center line to zero at solid boundaries. The contours between zero and ψ_{min} ($\psi_{\text{min}} < 0$) are also divided into equal increments, with the value of ψ_{min} given in the caption. All future contours will be presented in this way.

In the discussion to follow, the limit of creeping flow, where the inertial terms are removed from Equation (11), is considered. This limit is indicated as $Re_{\text{mod}} \rightarrow 0$.

Comparison Between the Mathematical Models

The ST-RT model is preferable to the RT-RT model because the former converges more rapidly and a smaller computer core is required. It was therefore important to establish the conditions for which the ST-RT model is a valid approximation for the RT-RT model.

Figure 3 shows the axial velocity profile at the expan-

Table 1. Ratio of Maximum Radial Velocity at $Z = 0$ to Maximum Radial Velocity in the Field from RT-RT Model as a Function of Re_{mod} for $n = 0.65$ and $n = 1.0$

n	Re_{mod}	Maximum radial velocity at $Z = 0$ / Maximum radial velocity in the field
0.65	0	0.465
0.65	5	0.165
0.65	10	0.081
0.65	20	0.050
1.00	0	0.580
1.00	5	0.361
1.00	10	0.122
1.00	20	0.056

sion mouth predicted by the RT-RT model. At $Re_{mod} \to 0$ the fluid has already decelerated in anticipation of the expansion while at $Re_{mod} = 10$ the deceleration is not nearly as marked. Predevelopment due to axial diffusion of momentum is obviously present at the lower Reynolds number flow, but this effect cannot be predicted using the ST-RT model. The magnitude of the radial component of velocity at the expansion mouth was found to be a sensitive indicator of predevelopment in the flow field. If no predevelopment occurs upstream of the plane of expansion, fully developed flow conditions exist at this plane and the radial velocity must be equal to zero. The deviation from zero can be thought of as a measure of the predevelopment. To normalize this indicator, we consider the ratio of the maximum velocity at $Z = 0$ to the maximum radial velocity in the field. Table 1 shows this ratio as a function of Re_{mod} for $n = 0.65$ and $n = 1$. Predevelopment, as measured by the deviation of the radial velocity ratio from zero, is greatest for the Newtonian fluid at $Re_{mod} \to 0$ (58%) and decreases rapidly until at $Re_{mod} = 20$, the ratio of the two velocities is less than 6%. Using the radial velocity ratio as a criterion for the use of the ST-RT model, it may be concluded that for $n \leq 1.0$, and $Re_{mod} \geq 20$, the ST-RT model is a good approximation for the RT-RT model.

The characteristics of the secondary flow were also found to be only mildly affected by the choice of model for $Re_{mod} \geq 20$. Table 2 shows the effect of each model on the reattachment length L/D and on the intensity of the secondary cell ψ_{min}. Also shown in Table 2 is the maximum value of the radial component of velocity in the field (U_{max}) as representative value of a sensitive velocity component in the bulk of the flow. The results of Table 2 confirm that the ST-RT model can be used confidently for $n \leq 1$ and for $Re \geq 20$. The flow patterns of Figure 2 also show that there is no substantial difference between the two models at $Re_{mod} = 20$.

Samuels and Wetzel (1972) measured the development of velocity at the center line of a submerged Newtonian planar jet and found that the fluid was unaware of the expansion for a Reynolds number greater than 40. They observed very small predevelopment of the center line velocity for Reynolds number greater than 10, but substantial predevelopment below 10. Although the results obtained in this work are for a different geometry and different boundary conditions, the Reynolds number criterion for the flow field to anticipate the change in cross-sectional area is in good agreement with the experimental work of Samuels and Wetzel.

Once the limits of applicability of the ST-RT and the RT-RT model were established, they were used to obtain the solutions in all cases for a 1 to 2 expansion with $0.65 \leq n \leq 1.0$ and $0 \leq Re_{mod} \leq 150$. These results are now discussed.

Secondary Cell Characteristics

Figure 4 shows the effect of the Reynolds number on the reattachment length (L/D) and on the intensity of the secondary cell (as characterized by the minimum value of the stream function, ψ_{min}) for three representative power-law indices. Also shown is the excellent agreement of this work with the results obtained by Hung (1966) for a Newtonian fluid with the same geometry.

The reattachment length increases monotonically with increasing Reynolds number. For $Re_{mod} < 40$, the relationship between (L/D) and Re_{mod} is almost linear for $n = 1.0$. As inertia becomes increasingly important (increasing Re_{mod}) the relationship deviates from linearity. For non-Newtonian fluids the nonlinearity becomes more pronounced, as the index n decreases from unity. This is probably caused by the variable nature of the apparent viscosity and of its derivatives in Equation (11).

The cell intensity is also a monotonic function of Reynolds number, increasing rapidly at low Reynolds numbers and approaching an asymptote at high Reynolds numbers. The increased intensity or circulation rate with Reynolds number results from an increased rate of momentum transfer from the bulk flow to the cell. However, the intensity does not increase without bound. If the cell intensity is bounded then so must be the energy dissipated at the wall in the region of the secondary cell, which is given by

$$\Lambda = \frac{64}{Re_{mod}} \int_0^l \tau_{RZ}|_{wall}\, dZ \qquad (44)$$

Λ can be determined from wall shear stress distribution

Table 2. Variation of Eddy Characteristics with Model

		ST-RT Model			RT-RT Model		
n	Re_{mod}	L/D	$-\psi_{min} \times 10^3$	U_{max}	L/D	$-\psi_{min} \times 10^3$	U_{max}
0.65	10	0.65	2.15	0.159	0.64	2.02	0.168
0.65	20	0.16	7.50	0.091	0.15	7.31	0.091
0.75	10	0.65	5.01	0.168	0.63	4.12	0.172
0.75	20	1.15	7.69	0.101	1.12	7.60	0.101
1.00	10	0.66	5.45	0.190	0.60	4.39	0.194
1.00	20	1.06	9.80	0.121	1.05	9.63	0.121

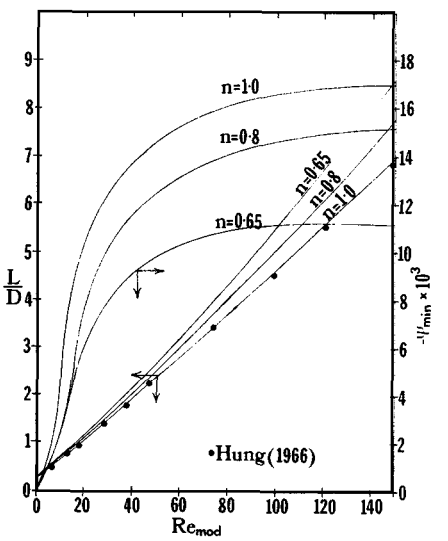

Fig. 4. Effect of Reynolds number on eddy characteristics.

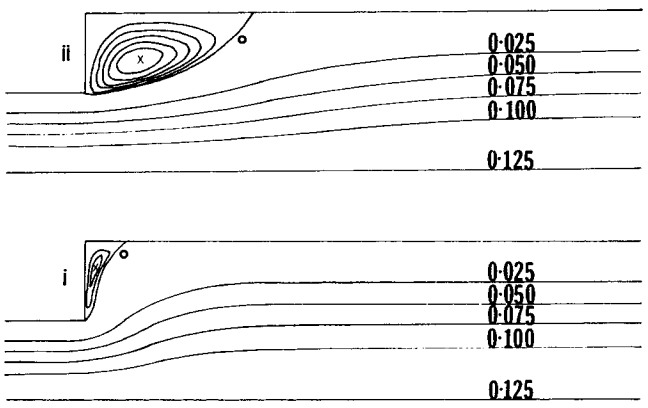

Fig. 5. Steam function contours for $n = 0.75$
(i) $Re_{mod} = 0$ $\psi_{min} = -0.00017$
(ii) $Re_{mod} = 20$ $\psi_{min} = -0.0061$

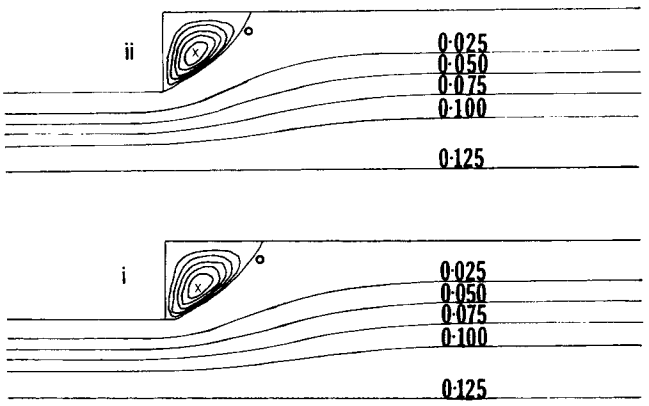

Fig. 6. Stream function contours for $Re_{mod} = 10$
(i) $n = 0.75$ $\psi_{min} = -0.00225$
(ii) $n = 1.0$ $\psi_{min} = -0.00263$

like that shown in Figure 12 for $n = 0.75$ and $Re_{mod} = 10$. Carrying out the graphical integration indicated by Equation (44) does indeed show that the energy dissipated at the wall in the region of the secondary flow approaches an asymptote at high Reynolds numbers. The integration limits are from the plane of expansion to the point where the stress field is 99% of its fully developed value.

Figure 5 illustrates the increasing size of the secondary cell which is associated with increasing values of the Reynolds number. As a result, the development length downstream of the expansion is also found to be longer for the larger value of the Reynolds number. The longer secondary cell allows the main flow to decelerate gradually and behaves not only as a dissipator of energy but also as a mechanism which shapes the flow through the expansion and dampens the effect of the discontinuity in geometry. In fact, it can be seen intuitively that the greater the inertia, the more difficult it is for the fluid to follow the contour of the expansion and, therefore, the larger will be the size of the cell. (We can also anticipate that the radial velocity near the expansion will be reduced.)

The effect of the power-law index on the flow field is illustrated in Figure 6 for a Reynolds number equal to 10 and for flow indices equal to 0.75 and 1.0, respectively. The secondary cell can be seen to be somewhat longer for the lower value of n. This effect, which is more clearly illustrated in Figure 4, is contrary to the trend observed by Giaquinta and Hung (1968) from their numerical solution of the equations describing the flow of a power-law through a planar expansion. The effect of n on the reattachment length is more dominant as the Reynolds number increases. For creeping flow, the reattachment length is 0.28 and is independent of power-law index (which compares well with the value of 0.27 quoted by Hung for $n = 1.0$). If the entrance length of Carter (1969) for flow of a power-law fluid through a sudden contraction and the reattachment length for this flow are considered as characteristic lengths of the respective flow fields, the independence of reattachment length from power-law index observed here at low Reynolds number agrees with the entry length results quoted by Carter.

The intensity of the secondary cell increases as n increases towards unity (Figure 4). This increase is caused by a reduction in the effective viscosity of the secondary motion as n tends to Newtonian behavior. The main flow is therefore able to drive the circulation in the cell at a higher rate. The effect of the power-law index on the intensity is again more pronounced at higher Reynolds numbers.

Velocity Fields

The axisymmetric flow produced by the sudden expansion can also be analyzed in terms of the axial and radial components of velocity. Both are functions of the Reynolds number and of the power-law index. Figure 7 is a typical solution which illustrates the development of the axial velocity profile for $n = 0.75$ and $Re_{mod} = 20$. As $Z \rightarrow -\infty$ the fully developed profile is imposed in the smaller pipe. The greatest deceleration takes place at the center line of the flow region: when $Z = 0.5$ (that is, 0.5 small tube

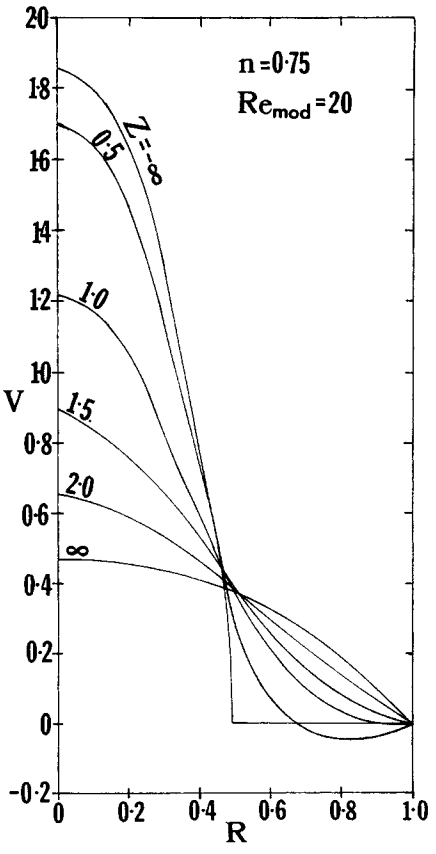

Fig. 7. Axial velocity profiles for different Z for $n = 0.75$, $Re_{mod} = 20$.

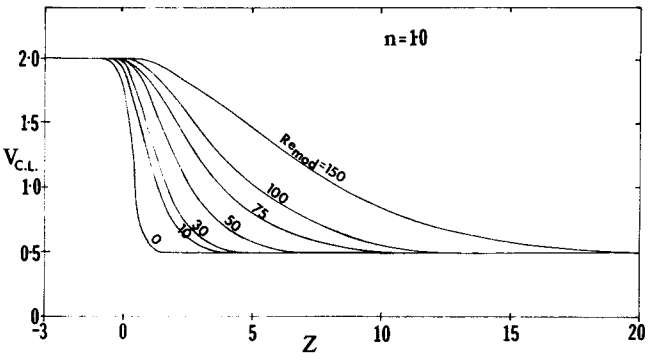

Fig. 8. Center line axial velocity development-variation with Reynolds number for $n = 1.0$.

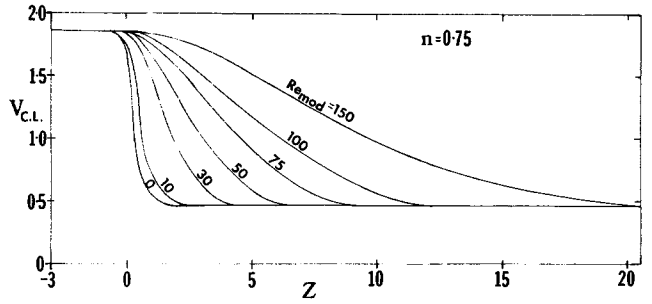

Fig. 9. Center line axial velocity development-variation with Reynolds number for $n = 0.75$.

diameters downstream of the plane of expansion), the center line velocity is reduced to 91% of the initial center line velocity. When $Z = 1.0$, 1.5 and 2.0, the center line velocity is reduced to 65%, 47%, and 35%, respectively, of the initial value. The final 10% reduction takes place from $Z = 2.0$ to $Z = \infty$. The change in axial velocity at any other radial plane is not as pronounced: when $R = 0.4$, the axial velocity at $Z = \infty$ is only 56% of the corresponding velocity in the small pipe. For this reason the dependence of the axial velocity on the two flow parameters (Re_{mod} and n) is best described by the center line values of this variable. Figures 8 and 9 show the distribution of axial velocity along the center line of the flow region for a range of values of the Reynolds number and for two values of the flow behavior index. The length necessary for fully developed flow to be reached increases with increasing Reynolds number: the secondary cell, at the higher Reynolds number, provides a surface which dampens the effect of the sudden expansion and allows a more gradual development. As the power-law index decreases ($n < 1.0$), the deceleration is less severe as a result of the longer cell. For example, at a Reynolds number of 150 and when $Z = 10$, the center line velocity is equal to 41% of the velocity in the small pipe for a Newtonian fluid but is equal to 53% of the corresponding velocity for the non-Newtonian fluid with $n = 0.75$.

The radial velocity in the fully developed region upstream of the expansion is equal to zero and, as fully developed flow is reached downstream, the radial velocity again becomes equal to zero. Typical profiles for $Re_{mod} = 10$ and $n = 0.75$ are shown in Figure 10. The radial velocity at the center line is equal to zero because of symmetry. The radii selected are such that the maximum value of the radial velocity (which occurs at $R = 0.4$) and the minimum value of the radial velocity (at $R = 0.6$) are both shown. Because of inertia effects and the presence of the eddy, the maximum radial velocity does not occur at $Z = 0$, but at a plane further downstream. As the Reynolds number increases, the inertia increases and the secondary cell lengthens, thus moving the location of the maximum radial velocity further downstream. The same effect is achieved when the power-law index is decreased ($n < 1.0$).

The minimum value of the radial velocity, a negative value, is found in the region of flow reversal, that is, where the liquid is flowing towards the center line. This minimum remains near the plane of expansion and shifts towards the bulk of the flow, or the expansion mouth, as the Reynolds number increases and as the power-law index decreases.

The variation in the value of the minimum radial velocity and in the value of the maximum radial velocity with Reynolds number is shown in Table 3.

The maximum radial velocity decreases with increasing Re_{mod} for both Newtonian and non-Newtonian liquids. This decrease is consistent with more gradual deceleration of the flow and with the buffering effect of the secondary cell. The minimum value of the radial com-

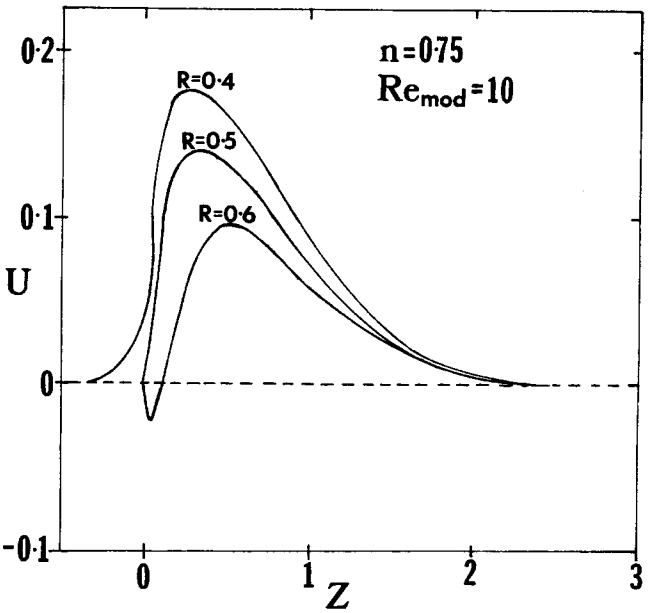

Fig. 10. Radial velocity profile for different radial planes for $n = 0.75$, $Re_{mod} = 10$.

Table 3. Variation of Extreme Values of the Radial Velocity Component with Re_{mod}

n	Re_{mod}	U_{max}	$U_{min} \times 10^3$
1.0	0	0.316	−4.00
1.0	10	0.194	−38.94
1.0	20	0.120	−51.77
1.0	30	0.086	−75.33
1.0	40	0.066	−79.28
1.0	50	0.054	−80.40
1.0	100	0.028	−75.39
1.0	150	0.018	−67.60
0.75	0	0.320	−0.48
0.75	10	0.169	−20.00
0.75	20	0.102	−60.00
0.75	30	0.071	−61.16
0.75	40	0.054	−63.81
0.75	75	0.076	−61.40
0.75	100	0.022	−58.24
0.75	150	0.015	−50.50

Table 4. Variation of Extreme Values of the Radial Velocity Component with the Power-Law Index

Re_{mod}	n	U_{max}	$U_{min} \times 10^3$
0	1.00	0.316	−4.00
0	0.90	0.322	−2.36
0	0.80	0.321	−0.78
0	0.75	0.320	−0.48
0	0.70	0.320	−0.23
0	0.65	0.318	−0.09
150	1.00	0.0189	−67.6
150	0.90	0.0169	−62.4
150	0.80	0.0154	−55.0
150	0.75	0.0147	−50.5
150	0.70	0.0140	−45.1
150	0.65	0.0139	−42.5

ponent of velocity is found to decrease with increasing Re_{mod} up to $Re_{mod} \simeq 40$ and then to increase gradually. This effect is a reflection of the increase in the intensity of the secondary cell and of the approach to an asymptotic value for $Re_{mod} > 40$.

The variation with the power-law index of the extreme values of the radial velocity component is shown for $Re_{mod} \rightarrow 0$ and 150 in Table 4.

The maximum radial velocity varies by less than 1% for creeping flow. This small variation is randomly distributed and can be attributed to truncation errors in the solution technique. At the higher Reynolds number, the maximum value of radial velocity decreases with decreasing values of the power-law index. This trend is consistent with the larger eddies.

The decrease in minimum radial velocity with decreasing n is caused by the increasing magnitude of the apparent viscosity at the near zero shear rates which are found in the secondary cell. As the cell becomes apparently more viscous, the motion of the eddy becomes more sluggish and smaller velocity components are observed.

Tanner (1973) solved the equations of motion for $n = 0.75$ and $Re_{mod} \rightarrow 0$ in a 2:1 expansion using a finite element technique. Several nodes that coincided with nodes in this work were compared for axial and radial velocities, as well as shear stresses. Excellent agreement was obtained.

Qualitative Description of the Stress Fields

The apparent viscosity and viscous stress components were calculated for each node once a converged solution was obtained. A complete set of contours for all the variables with a physical meaning is available (Halmos, 1973b) for $n = 0.75$ and $Re_{mod} = 10$.

The apparent viscosity, as expected, tends towards infinity at the three critical points discussed previously. In the region of the secondary cell, near the reattachment point, the apparent viscosity reaches a local maximum due to the near zero shear rate. Strictly, this too should be equal to infinity since a stagnation point occurs there. However, due to the finite difference technique used to evaluate this variable, infinity was not reached. Figure 11 shows the variation along the center line of the apparent viscosity for $n = 0.75$ and $Re_{mod} = 10$. The two extremes tend towards infinity and the minimum in the profile coincides with the plane of reattachment of the eddy. The greatest velocity gradients occur in this radial plane because the secondary cell is no longer damping the deceleration. Figure 11 also shows that the point at which the apparent viscosity is minimum coincides with the point at which the axial normal stress is maximum. The axial normal stress at the center line approaches zero for the fully developed flow regions and reaches a maximum at the plane of reattachment.

The shear stress encountered in the flow field is equal to zero at the center line and reaches a maximum when $R = \frac{1}{2}$ and $Z = 0$. In the secondary cell, the shear stress is acting back towards the 90° corner of the expansion. Therefore, at the point of reattachment, there is a sign change of the shear stress. Figure 12 shows the distribution of shear stress along the boundary ($R = 1.0$) for $n = 0.75$ and $Re_{mod} = 10$. The sign change occurs at the reattachment point and a minimum value is reached in the central plane of the eddy, that is, in the plane of minimum stream function.

Effect of Expansion Ratio

A few numerical solutions were obtained for varying expansion ratios (β). The study was limited to a Reynolds number of 10 due to the limitation in computer core. For $n = 0.75$ and $Re_{mod} = 10$ at an expansion ratio of 4, the size of field needed was 81 × 21 for a mesh size of

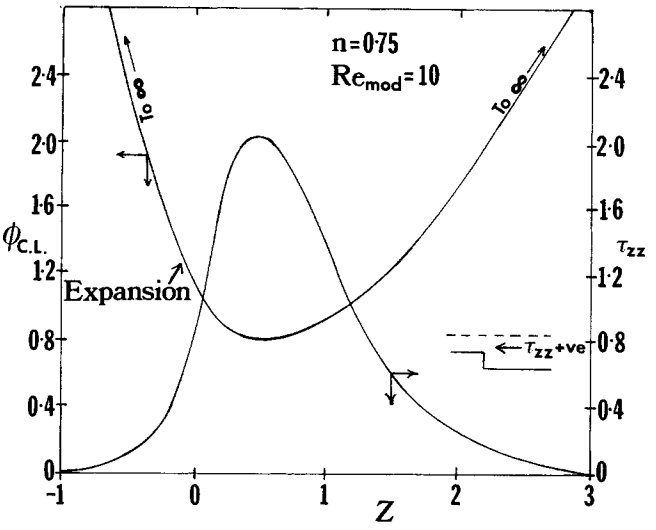

Fig. 11. Axial normal stress and apparent viscosity variation with axial position at the center line.

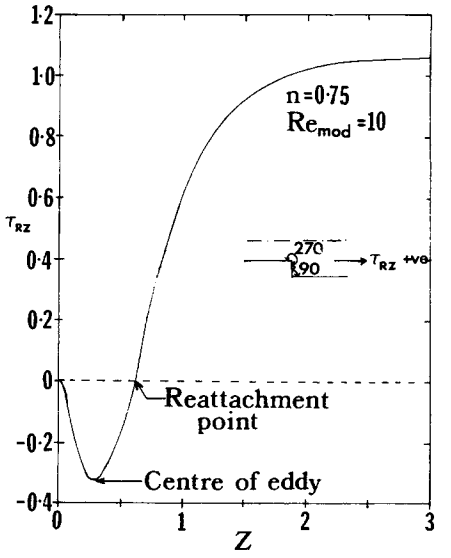

Fig. 12. Wall shear stress for $n = 0.75$ and $Re_{mod} = 10$.

Table 5. Expansion Ratio Effects

β	n	Re_{mod}	L/D	$-\psi_{min} \times 10^3$
1.5	1.0	10	0.31	1.56
2.0	1.0	10	0.66	5.45
3.0	1.0	10	1.28	13.70
4.0	1.0	10	1.89	22.90
2.0	0.9	10	0.65	4.57
3.0	0.9	10	1.28	11.00
4.0	0.9	10	1.92	17.20
2.0	0.75	10	0.65	2.80
3.0	0.75	10	1.29	7.84
4.0	0.75	10	1.99	12.00

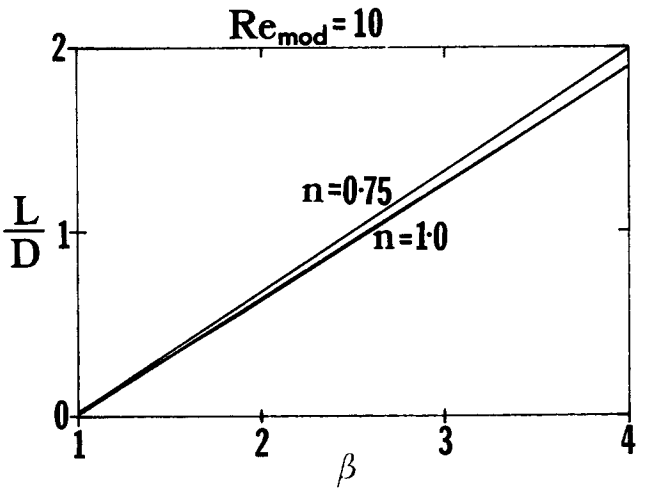

Fig. 13. Reattachment length dependence on expansion ratio for $Re_{mod} = 10$ with $n = 1.0$ and $n = 0.75$.

1/10 to reach fully developed conditions. Table 5 shows the variation of reattachment length and cell intensity with expansion ratio for a Newtonian and two non-Newtonian fluids with $n = 0.9$ and $n = 0.75$, respectively. The results obtained, although limited, show the trend of increasing reattachment length and intensity for increasing values of the expansion ratio.

Figure 13 shows that the reattachment length is a linear function of the expansion ratio in the range studied for both Newtonian and non-Newtonian ($n = 0.75$) fluids at a Reynolds number of 10. The range is not large enough to determine whether this linear relationship is universal, but the trend is certainly reliable. The increase in reattachment length for decreasing power-law index ($n \leq 1.0$) for $\beta > 2.0$ is consistent with the results obtained for $\beta = 2$.

The results indicate that for a higher expansion ratio, the trends with Re_{mod} and n observed for a 2 to 1 expansion will be similar, but the effects may be exaggerated because of greater deceleration.

ACKNOWLEDGMENTS

The authors are grateful to the Australian Research Grants Commission for their financial support and to B. Blake and P. J. Cable for their help in preparing the manuscript.

NOTATION

D = diameter of upstream tube
k = consistency index in power-law
L = length of secondary cell (dimensional)
n = power-law index (flow behavior index)
r = dimensional radial coordinate
R = dimensionless radial coordinate
U = dimensionless radial velocity
u, v = dimensional velocity components
V = dimensionless axial velocity
W = average upstream velocity
z = dimensional axial coordinate
Z = dimensionless axial coordinate

Greek Letters

β = expansion ratio
η = dimensionless vorticity
θ = dimensional azimuthal direction
Θ = dimensionless azimuthal direction
μ = Newtonian viscosity
ρ = density
τ'_{ij} = dimensional stress components
τ_{RZ} = dimensionless shear stress
$\tau_{ZZ}, \tau_{RR}, \tau_{\Theta\Theta}$ = dimensionless normal stress components (deviatoric)
ϕ = dimensionless apparent viscosity
ψ = dimensionless stream function
Λ = energy dissipated at the wall, Equation (44)

LITERATURE CITED

Bird, R. B., W. E. Stewart, and E. N. Lightfoot, *Transport Phenomena*, Wiley, New York (1960).

Cabelli, A., "A Numerical Study of the Benard Cell," Ph.D. thesis, Univ. of New South Wales, Sydney (1970).

Cabelli, A., and G. De-Vahl Davis, *J. Fluid Mech.*, **45**, 805 (1971).

Carter, T. R., "Laminar Flow From a Reservoir up to and Through a Tube-Entrance Region," Ph.D. thesis, Univ. Utah, Salt Lake City (1969).

Christiansen, E. B., S. J. Kelsey, and T. R. Carter, "Laminar Tube Flow Through an Abrupt Contraction," *AIChE J.*, **18**, 372 (1972).

Douglas, J., Jr., "Alternating Direction Methods for Three Space Variables," *Numerische Mathe.*, **4**, 41 (1962).

Giaquinta, A. R., and Tin-Kan Hung, "Slow Non-Newtonian Flow in a Zone of Separation," *J. Eng. Mech. Div.—Proc. Am. Soc. Civil Eng.*, 1521 (1968).

Halmos, A. L., "The Solution of the Equations of Motion for a Non-Newtonian Liquid Flowing Through a Sudden Expansion Using a Numerical Technique," Internal Report CHER 73-1, Monash Univ., Melbourne (1973a).

Halmos, A. L., "The Flow of Viscous and Viscoelastic Fluids Through an Abrupt Expansion," Ph.D. thesis, Monash Univ., Melbourne (1973b).

Hung, Tin-Kan, "Laminar Flow in Conduit Expansion," Ph.D. thesis, Univ. Iowa, Ames (1966).

Macagno, E. O., and Tin-Kan Hung, "Computational and Experimental Study of a Captive Cell," *J. Fluid Mech.*, **28**, 43 (1967).

Ozoe, H., and S. W. Churchill, "Hydrodynamic Stability and Natural Convection in Ostwald-de-Waele and Ellis Fluids: The Development of a Numerical Solution," *AIChE J.*, **18**, 1196 (1972).

Peaceman, D. W., and H. H. Rachford, Jr., "The Numerical Solution of Parabolic and Elliptic Differential Equations," *J. Soc. Ind. Appl. Maths.*, **3**, 28 (1955).

Prandtl, L., *Essentials of Fluid Mechanics*, Blackie & Sons, London (1963).

Samuels, M. R., and D. W. Wetzel, "Velocity Profiles in the Exit Region of a Submerged Jet," *Chem. Eng. J.*, **4**, 41 (1972).

Smith, G. P., *Numerical Solution of Partial Differential Equations*, Oxford Mathematical Handbook (1971).

Tanner, R. I., private communication.

Vrentas, J. S., J. L. Duda, and K. G. Bargeron, "Effect of Axial Diffusion of Vorticity of Flow Development in Circular Conducts: Part I, Numerical Solutions, *AIChE J.*, **12**, 837 (1966).

Manuscript received December 3, 1974; revision received January 28 and accepted January 29, 1975.